PRAMANA
— journal of
physics

Vol. 85, No. 2
August 2015
pp. 251–266

Dynamical features of nuclear fission

SANTANU PAL[1,2]
[1]CS-6/1, Golf Green, Kolkata 700 095, India
[2]Formerly with Variable Energy Cyclotron Centre, Kolkata 700 064, India
E-mail: santanupal1950@gmail.com

DOI: 10.1007/s12043-015-1040-6; ***e*Publication:** 24 July 2015

Abstract. It is now established that the transition-state theory of nuclear fission due to Bohr and Wheeler underestimates several observables in heavy-ion-induced fusion–fission reactions. Dissipative dynamical models employing either the Langevin equation or equivalently the Fokker–Planck equation have been developed for fission of heavy nuclei at high excitations ($T \sim 1$ MeV or higher). Here, we first present the physical picture underlying the dissipative fission dynamics. We mainly concentrate upon the Kramers' prescription for including dissipation in fission dynamics. We discuss, in some detail, the results of a statistical model analysis of the pre-scission neutron multiplicity data from the reactions ^{19}F+^{194,196,198}Pt using Kramers' fission width. We also discuss the multi-dimensional Langevin equation in the context of kinetic energy and mass distribution of the fission fragments.

Keywords. Fission; dissipation; Langevin equations; Fokker–Planck equation; Kramers' fission width.

PACS Nos 05.45.Gg; 24.60.Dr; 24.60.Lz; 24.75.+i; 25.70.Jj

1. Introduction

Experimental evidence accumulated over the last three decades indicates that the transition-state model of nuclear fission due to Bohr and Wheeler [1] is inadequate to describe the multiplicities of evaporated pre-scission light particles and photons [2–4] in heavy-ion-induced fusion–fission reactions. The standard statistical model of compound nuclear decay using the Bohr–Wheeler fission width is usually found to underpredict the pre-scission multiplicities beyond a certain threshold energy [5]. We first briefly re-visit the transition-state model to examine its underlying assumptions which may not be valid for fission at high excitation energies.

2. The transition-state model of fission

Let us consider an ensemble of nuclei in equilibrium. The fission rate according to the transition state model, often referred to as the statistical model of nuclear fission, is determined by the number of nuclei crossing the saddle configuration ('transition state') from the inside of the potential pocket. This outgoing flux depends on the density of states at the saddle configuration. The fission width then can be obtained as [1]

$$\Gamma_{\mathrm{BW}} = \frac{1}{2\pi\rho(E^*)} \int_0^{E^*-V_{\mathrm{B}}} \mathrm{d}\epsilon \rho^*(E^* - V_{\mathrm{B}} - \epsilon), \tag{1}$$

where E^* is the excitation energy and the other quantities are defined as shown in figure 1.

When $E^* \gg V_{\mathrm{B}}$, the above expression for fission width can be approximated as

$$\Gamma_{\mathrm{BW}} = \frac{T}{2\pi} \exp(-V_{\mathrm{B}}/T), \tag{2}$$

where the temperature T is related to E^* through the Fermi gas model. In 1973, Strutinsky [6] introduced a phase-space factor corresponding to the collective degrees of freedom in the ground-state region and consequently, the above approximate form of the Bohr–Wheeler fission width becomes

$$\Gamma_{\mathrm{BW}} = \frac{\hbar\omega_{\mathrm{g}}}{2\pi} \exp(-V_{\mathrm{B}}/T), \tag{3}$$

where ω_{g} is the frequency of a harmonic oscillator potential which represents the nuclear potential near the ground state.

One important assumption in the transition-state model is that of equilibration at each instant during the fission process. This assumption is expected to be valid when the flux across the fission barrier is very small or in other words, the fission barrier is much larger than the temperature. However, for systems with lower fission barriers and/or high excitation energies, there may not be sufficient nuclei near the fission barrier after the

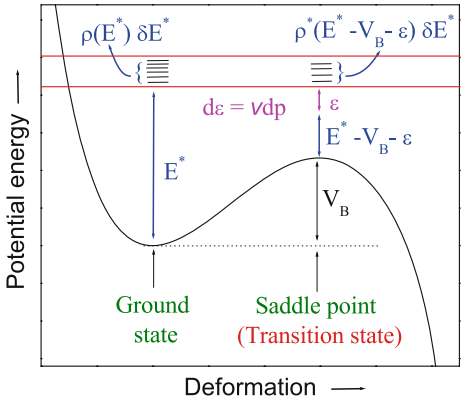

Figure 1. A schematic representation of the Bohr–Wheeler theory of fission.

initial crossings are made [7]. In order to maintain a steady flux across the barrier, it thus becomes essential to consider a dynamical model of fission.

3. A dissipative dynamical model of nuclear fission

In nuclear fission, a nucleus evolves from a relatively compact mononuclear shape to a dinuclear configuration. This shape evolution is caused by the interaction between the nuclear collective coordinates (which specify the nuclear shape and are a few in number) with the rest of the nuclear intrinsic degrees of freedom. The interaction between the collective and the intrinsic degrees of freedom gives rise to a dissipative force in the equation of collective motion averaged over an ensemble of nuclei [8,9]. Further, the interaction term for individual nuclei in the ensemble depends upon a large number of intrinsic coordinates and hence can be represented by a fluctuating force in the collective motion. The fission dynamics thus is very similar to that of a massive Brownian particle floating in an equilibrated heat bath placed in a potential field. The heat bath here represents the motion associated with the intrinsic degrees of freedom of the nucleus and the potential energy is the deformation energy of the nucleus. The fission dynamics is thus both dissipative and diffusive (due to the fluctuating force) in nature and the equation of motion, known as the Langevin equation, is given in one dimension as

$$\frac{\mathrm{d}p}{\mathrm{d}t} = -\frac{\mathrm{d}V}{\mathrm{d}q} - \eta\frac{\mathrm{d}q}{\mathrm{d}t} + R(t),$$
$$\frac{\mathrm{d}q}{\mathrm{d}t} = \frac{p}{m}, \tag{4}$$

where (q, p) are, respectively the collective fission coordinate and the conjugate momentum, V is the collective potential, m is the collective inertia and η is the dissipation coefficient. The fluctuating force is represented by $R(t)$ which can be suitably modelled using the fluctuation–dissipation theorem [10,11].

It should be noted that the Langevin equation is different from ordinary differential equations as it contains a stochastic term $R(t)$. To calculate the physical quantities such as the mean values or the distributions of observables from such a stochastic equation, one has to deal with a sufficiently large ensemble of trajectories for a true realization of the stochastic force. The physical description of the Brownian motion is therefore contained in a large number of stochastic trajectories rather than in a single trajectory, as would be the case for the solution of a deterministic equation of motion.

An alternative but equivalent description of stochastic dynamics can be obtained by considering the total ensemble of Langevin trajectories. The time evolution of the ensemble can be viewed as a diffusion process in a collective phase-space [7]. The corresponding diffusion equation, the Fokker–Planck equation, in one dimension and in steady state is given as

$$p\frac{\partial\rho}{\partial q} - \frac{\mathrm{d}V}{\mathrm{d}q}\frac{\partial\rho}{\partial p} = \eta\frac{\partial(p\rho)}{\partial p} + \eta T\frac{\partial^2\rho}{\partial p^2}, \tag{5}$$

where ρ is the distribution function of the ensemble. Kramers [7] solved the one-dimensional Fokker–Planck equation to obtain the stationary current of the Brownian

particles over a potential barrier and the fission width is subsequenly obtained as

$$\Gamma_{\mathrm{K}} = \frac{\hbar\omega_{\mathrm{g}}}{2\pi} \exp\left(-V_{\mathrm{B}}/T\right) \left\{ \sqrt{1 + \left(\frac{\beta}{2\omega_{\mathrm{s}}}\right)^2} - \frac{\beta}{2\omega_{\mathrm{s}}} \right\}, \tag{6}$$

where $\beta = \eta/m$ and ω_{s} denotes the frequency of an inverted harmonic oscillator potential which approximates the nuclear potential in the saddle region. The above width, often referred to as the Kramers' fission width, can be used as the fission width in the decay of an excited compound nucleus.

The validity of the Kramers' fission width can be tested by comparing it with the fission width obtained from numerical simulation of the Langevin equation. One such comparison is shown in figure 2 [12]. It is observed that the Kramers' width and the stationary width from the Langevin dynamical calculation are in close agreement when $V_{\mathrm{B}} > T$, which is the domain of validity of the Kramers' expression.

The main advantage of the Kramers' width is that it can be easily implemented in a statistical model code of compound nuclear decay. Thus, one can study the effects of dissipation in nuclear fission using a statistical model code instead of solving the Langevin or Fokker–Planck equations. The strength of the dissipation coefficient β is usually treated as an adjustable parameter in order to fit the experimental data. The results of one such study is discussed in the following section.

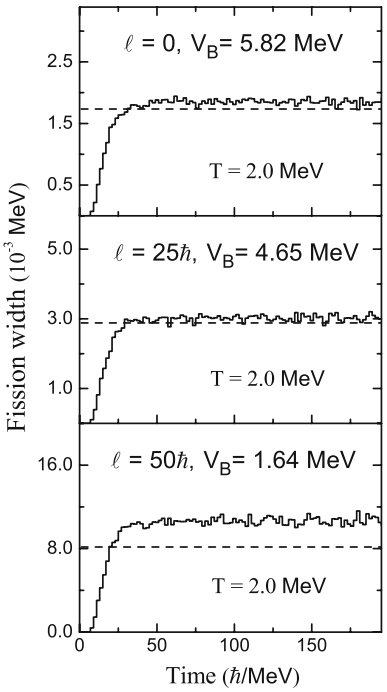

Figure 2. Time-dependent fission widths (——) from Langevin equation for different values of spin (ℓ) of ^{224}Th at a temperature of 2 MeV. (- - - -) The corresponding values of Kramers' width.

4. Statistical model analysis of ^{19}F+^{194,196,198}Pt reactions

Dissipation in nuclear dynamics in the mean-field regime accounts for the coupling of the collective motion with the intrinsic nucleon degrees of freedom. The energy spectra of intrinsic motion has a well-defined shell structure which is known to persist in an excited nucleus [13–16]. It is therefore of considerable interest to investigate the effect of shell structure on the strength of nuclear dissipation. Guided by the above considerations, an experiment was performed to explore the effect of shell closure on nuclear dissipation through the pre-scission neutron multiplicity ($M_{\rm pre}$) measurement [17,18]. Three different isotopes of Fr were populated through fusion of the ^{19}F projectile with the ^{194,196,198}Pt target nuclei. Out of the compound nuclei, ^{213}Fr contains neutron shell closure ($N = 126$) and the other two are away from shell closure. The compound nuclei were formed in the excitation energy range of 46.6–91.8 MeV.

Statistical model analysis of the above experimental data was performed by considering the evaporation of neutrons, protons, α-particles and the statistical giant dipole γ-rays as the compound nuclear decay channels, in addition to fission [17,18]. The intensity of different decay modes depends critically on the density of levels of the parent and the daughter nuclei. The level density in turn is a sensitive function of the level-density parameter (a) which was taken from the work of Ignatyuk *et al* [19], who proposed a form which includes the shell effects at low excitation energies and goes over to its asymptotic form at high excitation energies and is given as follows:

$$a(E^*) = \bar{a}\left(1 + \frac{f(E^*)}{E^*}\delta W\right) \tag{7}$$

with

$$f(E^*) = 1 - \exp(-E^*/E_d), \tag{8}$$

where $\bar{a}$ is the asymptotic level density and E_d is a parameter which decides the rate at which the shell effects disappear with increase in the excitation energy (E^*). A value of 18.5 MeV was used for E_d which was obtained from the analysis of s-wave neutron resonances [20]. The shell correction term δW is given as the difference between the experimental and liquid-drop model (LDM) masses ($\delta W = M_{\rm exp} - M_{\rm LDM}$). The asymptotic level density $\bar{a}$ was taken from [20].

In the Kramers' fission width eq. (6), shell effect is taken into account by modifying the fission barrier as [19]

$$V_{\rm B}(T) = V_{\rm LDM} - \delta W \exp(-E^*/E_d), \tag{9}$$

where $V_{\rm LDM}$ is the fission barrier from the finite-range rotating liquid drop model (FRLDM) potential [21].

Taking into account the shell effects in the level densities and the fission barriers, the pre-scission neutron multiplicity, $M_{\rm pre}$, at each excitation energy was fitted with the statistical model calculation using β as a free parameter and figure 3a shows the results [17]. The corresponding values of β are given in figure 3b. In this plot, the shaded area for each nucleus accounts for the uncertainty in the fitted β values owing to the error in the experimental $M_{\rm pre}$ values.

It is observed that β values for ^{215}Fr and ^{217}Fr are remarkably close within the limits of uncertainty over the entire excitation energy range. The shell structures of the

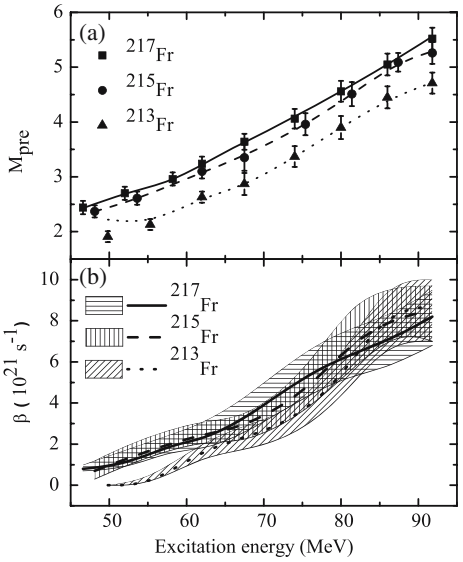

Figure 3. (**a**) Experimental pre-scission neutron multiplicity (symbols) for different systems with statistical model fits (lines) when shell effects are included in the calculation. (**b**) Best-fit values (lines) of β. Hatched areas represent the uncertainty in β associated with the experimental error in $M_{\rm pre}$.

above two isotopes of Fr are also very similar, each having a partially occupied $1g_{9/2}$ neutron shell after the shell gap at neutron number 126. On the other hand, the dissipation strength required for ^{213}Fr is clearly smaller than those for ^{215}Fr and ^{217}Fr at lower excitation energies though all the three become close at higher excitation energies. With a major shell closure with 126 neutrons, the shell structure of ^{213}Fr is very distinct from those of ^{215,217}Fr. Recalling that the shell structure can influence level density, fission barrier as well as the strength of dissipation, the above observation regarding smaller dissipation for ^{213}Fr can solely be attributed to its shell structure, because shell effects in the level density and the fission barrier are already included in the calculation. We thus arrive at the following conclusion regarding shell effect on dissipation. While the reduced dissipation strength varies marginally among nuclei which are away from shell closure, it is suppressed for shell closure nuclei at low excitations. This feature can also be expected from the microscopic theories of one-body dissipation [8,22], where the incoherent particle–hole excitation by a time-dependent mean field causes dissipation. Particle–hole excitation being easier for non-closed shell nuclei than for closed shell nuclei, the former is expected to be more dissipative than the latter. The present results provide a phenomenological evidence for this expectation.

We also observe a strong (initial) excitation energy dependence of β in figure 3b. Though the excitation energy dependence of nuclear dissipation is not yet clearly understood, it is usually attributed to several factors which include neglect of higher-order terms in microscopic derivations of dissipation [23], shape dependence of dissipation [4], inadequacies in fission modelling [24] and need for a better treatment of the inertia [16]. We, however, feel that inclusion of the above effects in nuclear dissipation will not alter the

relative strengths of dissipation of different nuclei at each excitation energy and the shell closure effects will persist.

Statistical model calculations were next performed without considering shell effects [17] and figure 4 shows the best-fit M_{pre} and the corresponding β values. It is curious to observe that M_{pre} cannot be fitted at all at low excitation energies for all the three Fr isotopes. It is further observed that the best-fit β values for different isotopes are quite different in contrast to those obtained with shell effects as given in figure 3. To seek an explanation for this behaviour, the nature of the neutron width with and without the shell correction was examined [17]. As the neutron width is essentially determined by the ratio of the level densities of the daughter and the parent nuclei, inclusion of shell correction increases or decreases the neutron width depending upon the relative magnitudes of the shell correction in the daughter and the parent nuclei.

As a consequence of the systematic variation of shell correction for the Fr isotopes across the shell closure at $N = 126$ (inset of figure 5), it was observed [17] that Γ_n and Γ_n/Γ_f get modified as illustrated in figure 5. Increase of Γ_n/Γ_f ratio for $^{214-217}$Fr results in the enhancement of neutron multiplicity for ^{217}Fr when shell effects are not included in the calculation. The enhancement is so pronounced at lower excitation energies that even the largest fission width with β=0 cannot reproduce the experimental multiplicity in figure 4. This enhancement also reduces the best-fit β values in comparison to those in figure 3 at higher excitation energies for ^{217}Fr. On the other hand, decrease of the Γ_n/Γ_f ratio for ^{212}Fr and lighter isotopes causes suppression of neutron multiplicity for ^{213}Fr, which in turn demands a stronger fission hindrance in order to fit the experimental data. Therefore, the fitted β values are much larger than the values obtained with shell effect. For ^{215}Fr, the Γ_n/Γ_f ratio increases for some and decreases for other Fr compound nuclei which are encountered during the successive neutron emissions. The β values for ^{215}Fr

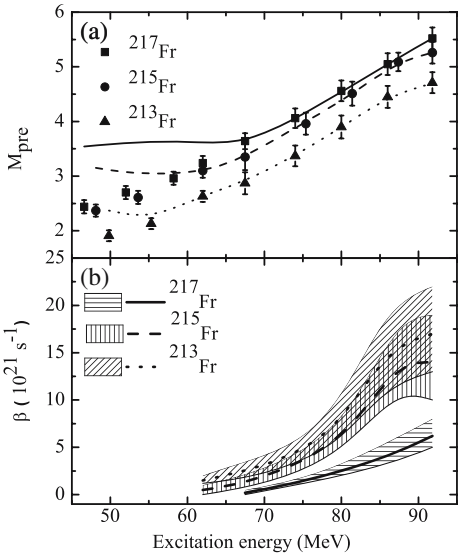

Figure 4. Same as figure 3 except that the statistical model calculations were performed by excluding the shell effects.

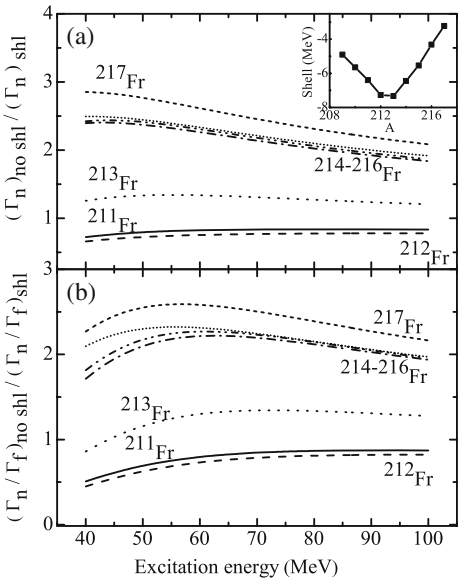

Figure 5. (**a**) Comparison of neutron widths with and without shell effects for different isotopes of Fr. (**b**) Similar comparison for the neutron-to-fission width ratio. The widths are calculated for compound nuclei with spin $40\hbar$. Inset shows the variation of shell correction with mass number for Fr isotopes.

therefore, lie in between those of ^{213}Fr and ^{217}Fr. Thus, the large variation of β among the three nuclei can be attributed to the neglect of shell effects. This, in turn, establishes the importance of the inclusion of shell effects in statistical model calculations to obtain a consistent picture of nuclear dissipation.

The role of neutron binding energy in neutron multiplicity was examined in [18] by performing statistical model calculations using LDM nuclear masses to obtain the neutron binding energies and FRLDM for the fission barrier. Shell corrections were not applied either to the neutron binding energies or to the fission barrier. The pre-scission neutron multiplicity at each excitation energy was fitted by adjusting the strength of the reduced dissipation coefficient β. Figure 6 shows the best-fit β values for different isotopes of Fr. It is observed that the dissipation coefficients for ^{217}Fr and ^{215}Fr isotopes increase rapidly with increasing excitation energy over its entire range, whereas the dissipation strength remains nearly zero till 70 MeV of excitation energy followed by a slower rate of increase for ^{213}Fr. The overall magnitude of the dissipation strength also remains much smaller for ^{213}Fr than for the other two isotopes of Fr.

Ground-state shell corrections in the LDM masses were subsequently incorporated in the statistical model calculations [18]. Figure 7 shows the dissipation strengths required to fit the experimental multiplicities for all the three Fr isotopes. It is clearly observed in figure 7 that the anomalous lowering of dissipation strength for ^{213}Fr disappears and all the isotopes require nearly the same dissipation strength to fit the experimental results. This observation can be explained as follows. As the masses are considered to be the sum of the LDM masses and the shell corrections, the neutron separation energy obtained from the shell-corrected LDM masses increases for ^{213}Fr compared to that from the LDM masses

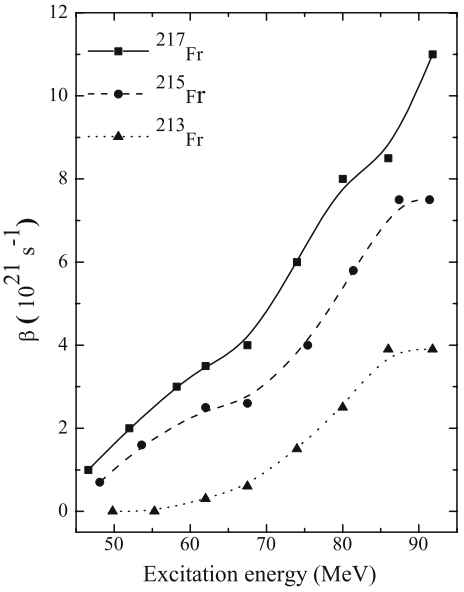

Figure 6. Excitation energy dependence of β required to fit the experimentally obtained M_{pre} for different systems using LDM and without shell correction in fission barrier. The lines are drawn to guide the eye.

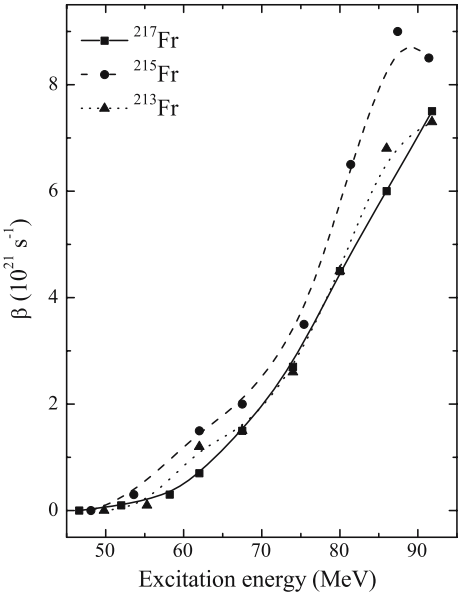

Figure 7. Excitation function of β values required to fit experimentally the obtained M_{pre} using the shell-corrected LDM mass and without shell correction in fission barrier for different isotopes of Fr. The lines are drawn to guide the eye.

while it decreases for the other two isotopes. This reduces the $M_{\rm pre}$ values for ^{213}Fr, but increases the same for ^{217}Fr and ^{215}Fr for a given value of the dissipation strength in the statistical model calculations. Consequently, higher values of dissipation strength are required to fit $M_{\rm pre}$ for ^{213}Fr whereas lower values of dissipation are required for the other two isotopes, in comparison to the calculations without shell correction in masses. The dissipation strengths of the different isotopes therefore converge.

The LDM masses with shell corrections however differ from the experimental ground-state masses to some extent. Hence, the experimental ground-state nuclear masses were used in the statistical model calculations [18]. Figure 8 shows the fitted β values for the three isotopes of Fr. Here also we find the excitation functions of the fitted β values to be nearly the same for all the three Fr isotopes.

Comparing the results given in figures 6, 7 and 8, an interesting observation is made here. When shell correction is not applied to the ground-state nuclear masses, the fitted β values for the different Fr isotopes are quite different (figure 6). However, the best-fit β values for the three Fr isotopes converge to a common value at each excitation energy when either shell-corrected (figure 7) or experimental nuclear masses (figure 8) are used in the statistical model calculations.

The effect of shell correction to the fission barrier on the fitted values of dissipation strength was investigated next [18]. To this end, the excitation functions of the fitted β obtained without shell correction to fission barrier (figure 8) are compared with those obtained with shell-corrected fission barrier (figure 9). Experimental nuclear masses are used in both the calculations. It is observed that inclusion of shell effects in fission barrier affects the fitted β values differently for shell-closed and non-shell-closed nuclei at low

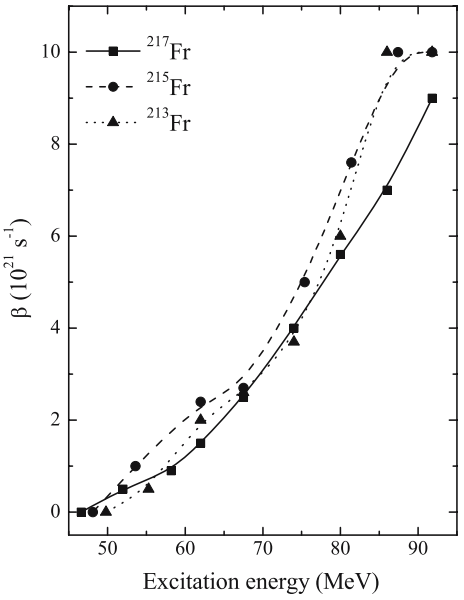

Figure 8. Excitation function of β values required to fit experimentally the obtained $M_{\rm pre}$ using the experimental mass and without shell corrections in fission barrier for different isotopes of Fr. The lines are drawn to guide the eye.

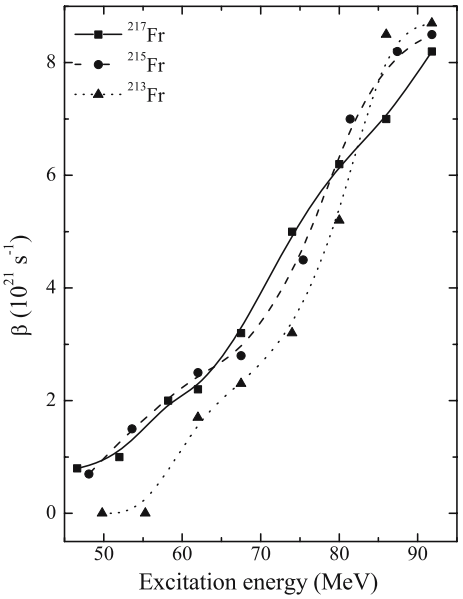

Figure 9. Excitation function of β values required to fit experimentally obtained M_{pre} using the experimental mass and shell-corrected fission barrier for different isotopes of Fr. The lines are drawn to guide the eye.

excitation energies. However, the effect of inclusion of shell correction in fission barrier is not as severe as the effect of shell correction in LDM masses (figures 6 and 7) or the effect of shell correction in the level density formulas [17].

5. Multidimensional Langevin equation

Though the statistical model of nuclear decay with Kramers' fission width can reproduce pre-scission multiplicities of light particles and photons, a multidimensional dynamical equation is required to obtain the fission fragment mass and kinetic energy distributions. The fragment mass and kinetic energy distributions are determined to a large extent by the potential energy profile along the saddle ridge in a multidimensional potential landscape. Though one can obtain the fragment distribution along the saddle ridge by assuming an equilibrated configuration [25,26], it is evidently more desirable to get it from a dynamical model. In the descent from the saddle ridge to the scission configuration, the fission fragment mass and kinetic energy distributions can evolve further which can be followed through a dynamical equation. Multidimensional Langevin equation has been employed by several researchers to study fission fragment mass and kinetic energy distributions [27,28].

The multidimensional Langevin equation has the following form [29]:

$$\frac{\mathrm{d}p_i}{\mathrm{d}t} = -\frac{p_j p_k}{2}\frac{\partial}{\partial q_i}(m^{-1})_{jk} - \frac{\partial V}{\partial q_i} - \eta_{ij}(m^{-1})_{jk}p_k + g_{ij}\Gamma_j(t),$$
$$\frac{\mathrm{d}q_i}{\mathrm{d}t} = (m^{-1})_{ij}p_j, \tag{10}$$

where q_i stands for the collective coordinates and p_i represents the respective momentum, V is the potential energy of the system and m_{ij} and η_{ij} are the shape-dependent collective inertia and dissipation tensors, respectively. The strength of the random force is related to the dissipation coefficients through the fluctuation–dissipation theorem and is given as

$$g_{ik}g_{jk} = \eta_{ij}T, \tag{11}$$

where T is the temperature of the compound nucleus. Usually, the one-body wall plus window model of nuclear dissipation [23] is used in Langevin dynamical calculations.

In what follows, the collective coordinates will be taken as the 'funny hills' shape parameters (c, h, α'), where the symbols represent the elongation, neck and the mass asymmetry of a nucleus, respectively [30]. A two-dimensional contour plot of finite-range LDM potential of ^{224}Th is shown in figure 10 [31].

The Langevin equation in elongation and neck coordinates were numerically solved in [3] using the potential given in figure 10 and the kinetic energy distributions of the fission fragments were obtained by assuming symmetric fission (figure 11). The kinetic energy distributions obtained in one dimension (with only elongation coordinate) are also shown in figure 11. It is observed that the two-dimensional fission trajectories give rise to fission fragment kinetic energy distributions which are distinct from those obtained in one-dimensional motion. As the potential energy at scission is the same for all the trajectories in one dimension, the Boltzmann-like distribution indicates a near-equilibration at scission. On the other hand, the potential energy at scission can be different for different two-dimensional trajectories which, in turn, results in a kinetic energy distribution which is more symmetric than the one-dimensional distribution. One can also expect that the dispersion of potential energy at scission would further increase with the addition of more degrees of freedom resulting in a broader and more symmetric distribution. Experimental fission fragment kinetic energies displaying Gaussian distributions therefore suggest a multidimensional dynamics of fission.

We further note in figure 11 that the peak appears at a lower energy for two-dimensional motion compared to that in one dimension. This aspect essentially reflects the fact that a nucleus with (c, h) degrees of freedom is more elongated at scission than the one with

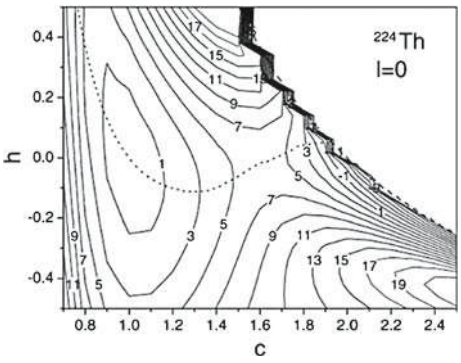

Figure 10. Potential energy contours (in MeV) in elongation (c) and neck (h) coordinates for ^{224}Th. The minimum in the potential energy valley is marked by the dotted line. The dashed line corresponds to scission configuration.

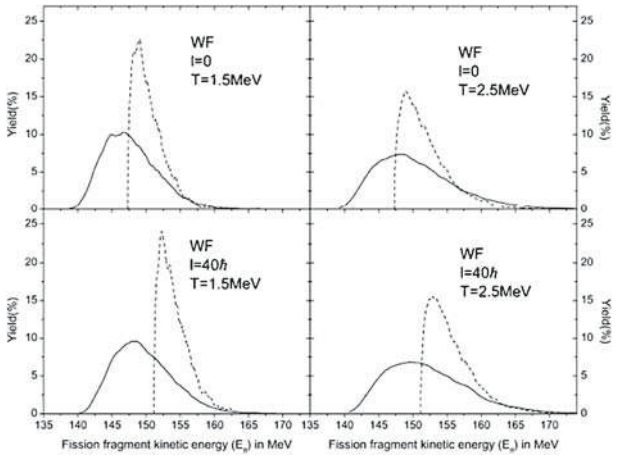

Figure 11. Fission fragment kinetic energy distribution calculated with wall friction (WF) at different spins and temperatures of ^{224}Th. The yield of fission fragments in % (y-axis) is plotted against the kinetic energy of the fission fragments in MeV (x-axis). The solid and dotted lines are obtained from calculations in two and one dimensions, respectively.

only c degree of freedom. This results in a lower Coulomb barrier and hence a smaller kinetic energy of the fission fragments for the former case compared to the latter.

Another example of a two-dimensional potential landscape is shown in figure 12, where elongation (c) and asymmetry (α') are considered as the relevant coordinates [32]. The mass asymmetry parameter α' is related to the ratio of masses of the nascent fragments A_1 and A_2 as

$$\frac{A_1}{A_2} = \frac{1 + \frac{3}{8}\alpha'}{1 - \frac{3}{8}\alpha'}. \tag{12}$$

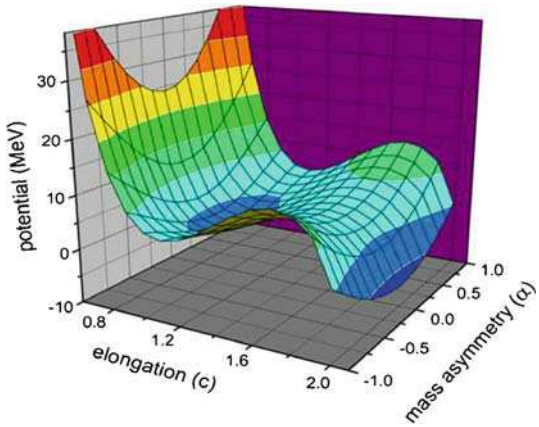

Figure 12. The potential energy landscape in elongation and mass asymmetry coordinates for ^{224}Th.

Table 1. Z^2/A, saddle-to-scission distance c_{SS} (in unit of compound nuclear radius) and fission barrier (V_B) for symmetric fission of several compound nuclei.

	^{124}Ba $\ell = 60\hbar$	^{184}W $\ell = 60\hbar$	^{208}Pb $\ell = 60\hbar$	^{206}Po $\ell = 60\hbar$	^{224}Th $\ell = 60\hbar$	^{254}Fm $\ell = 40\hbar$
Z^2/A	25.29	29.76	32.33	34.25	36.16	39.37
c_{SS}	0.08	0.14	0.32	0.46	0.63	0.74
V_B (MeV)	8.61	8.63	3.41	1.76	0.38	0.10

Numerical solutions of the Langevin equation in (c, α') coordinates were obtained with a view to study the role of saddle-to-scission dynamics in fission [32]. We shall briefly discuss here some of the results obtained in [32]. In addition to the (wall+window) dissipation, another dissipation term γ^{asym} associated with the rate of change of time of mass asymmetry degree of freedom [33] was considered in [32]. Calculations were performed for a number of nuclei with spin values so chosen that they represent a broad range of saddle-to-scission distances and also a range of fission barriers as given in table 1.

In a Langevin dynamical calculation, a fission trajectory can cross the saddle ridge many times in a to-and-fro motion before it reaches the scission line. Accordingly, the asymmetry coordinates corresponding to the last crossing of the saddle ridge by the fission trajectories were used to obtain the mass variance at the saddle and those corresponding to the crossing of the scission line gave the mass variance at scission. Mass variances were obtained with and without the term γ^{asym} in the calculation.

The distribution of fission fragment mass were initially calculated without the γ^{asym} term and the corresponding mean-square deviations σ_m^2 for the different systems were obtained as shown in figure 13. It is observed that the mass variance of a system decreases as it moves from the saddle to the scission region. As γ^{asym} was not included in the calculation of mass variance in figure 13, a strong dissipative force was absent in the saddle-to scission dynamics. Therefore, the funnel shape of the potential landscape in the saddle-to-scission region pushes the system towards a symmetric configuration and consequently, the mass variance at scission decreases.

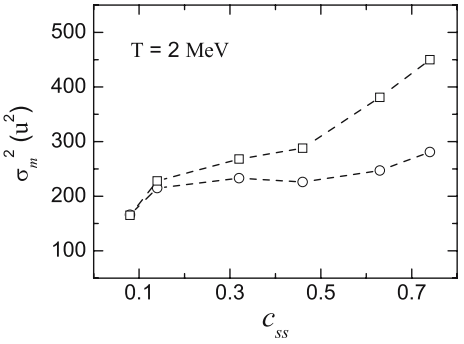

Figure 13. The mass variances σ_m^2 at the saddle ridge (□) and on the scission line (○) as a function of the saddle-to-scission distance from dynamical model calculation without the γ^{asym} term. Lines are drawn to guide the eyes.

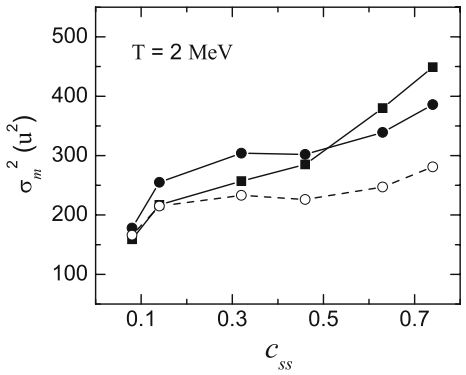

Figure 14. The mass variances σ_{m}^2 calculated with (●, ■) and without (○) the γ^{asym} term for different systems. The circles and squares represent the variances at scission and saddle, respectively. The variances at the saddle with and without γ^{asym} are nearly the same and are indistinguishable in the plot. Lines are drawn to guide the eyes.

The mass variances were subsequently obtained with γ^{asym} in the Langevin dynamical calculations and are shown in figure 14. Dynamical model results without γ^{asym} (as given in figure 13) are also shown in this figure for comparison. The variances at the saddle obtained with and without γ^{asym} are indistinguishable in this figure, which is expected because γ^{asym} becomes effective only beyond the neck line. It is observed in this figure that the variances at scission are enhanced with the inclusion of γ^{asym} in the calculation. This is a consequence of the random force associated with γ^{asym}, which operates between the neck line and the scission line and drives the system towards larger asymmetry, thus demonstrating the importance of the asymmetry term in the generalized one-body dissipation.

A large volume of experimental data has been analysed in recent years by employing three-dimensional Langevin equation [28,34–37]. It is observed in all such analyses that a reduction of the strength of one-body wall dissipation is required to fit the data. It is also observed that different strengths of dissipation are required to fit different types of experimental data. Evidently, further investigations are necessary to resolve such issues in future works.

6. Summary and outlook

In summary, we have discussed the dissipative dynamical nature of heavy-ion-induced fusion–fission reactions. It has been pointed out that while dissipation can be taken into account in statistical model calculations by using the fission width due to Kramers to calculate pre-scission multiplicities of evaporated particles, multidimensional Langevin dynamical calculations are essential for calculating fission fragment mass and kinetic energy distributions. Though considerable progress has been made in understanding the dynamical features of nuclear fission, testing of the dynamical models with inputs from microscopic models are yet to be performed. The role of isospin degree of freedom in fission is also expected to be investigated in detail from fusion–fission experiments with

unstable beams. Thus, development of a dynamical fission model with isospin degree of freedom is expected to be addressed in future works.

References

[1] N Bohr and J A Wheeler, *Phys. Rev.* **56**, 426 (1939)
[2] D J Hinde, R J Charity, G S Foote, J R Leigh, J O Newton, S Ogaza and A Chattejee, *Nucl. Phys. A* **452**, 550 (1986)
[3] J O Newton, D J Hinde, R J Charity, R J Leigh, J J M Bokhorst, A Chatterjee, G S Foote and S Ogaza, *Nucl. Phys. A* **483**, 126 (1988)
[4] I Dioszegi, N P Shaw, I Mazumder, A Hatzikoutelis and P Paul, *Phys. Rev. C* **61**, 024613 (2000)
[5] M Thoennessen and G F Bertsch, *Phys. Rev. Lett.* **71**, 4303 (1993)
[6] V M Strutinsky, *Phys. Lett. B* **47**, 121 (1973)
[7] H A Kramers, *Physica (Amsterdam)* **7**, 284 (1940)
[8] H Hofmann and P J Siemens, *Nucl. Phys. A* **257**, 165 (1976)
[9] S E Koonin and J Randrup, *Nucl. Phys. A* **289**, 475 (1977)
[10] P Fröbrich and I I Gontchar, *Phys. Rep.* **292**, 131 (1998)
[11] Y Abe, S Ayik, P-G Reinhard and E Suraud, *Phys. Rep.* **275**, 49 (1996)
[12] J Sadhukhan and S Pal, *Phys. Rev. C* **79**, 064606 (2009)
[13] J L Egido, L M Robledo and V Martin, *Phys. Rev. Lett.* **85**, 26 (2000)
[14] J C Pei *et al*, *Phys. Rev. Lett.* **102**, 192501 (2009)
[15] A V Ignatyuk *et al*, *Nucl. Phys. A* **346**, 191 (1980)
[16] F A Ivanyuk and H Hofmann, *Nucl. Phys. A* **657**, 19 (1999)
[17] Varinderjit Singh *et al*, *Phys. Rev. C* **86**, 014609 (2012)
[18] Varinderjit Singh *et al*, *Phys. Rev. C* **87**, 064601 (2013)
[19] A V Ignatyuk *et al*, *Yad. Fiz.* **21**, 485 (1975), [*Sov. J. Nucl. Phys.* **21**, 255 (1975)]
[20] W Reisdorf, *Z. Phys. A* **300**, 227 (1981)
[21] A J Sierk, *Phys. Rev. C* **33**, 2039 (1986)
[22] S Pal and N K Ganguly, *Nucl. Phys. A* **370**, 175 (1981)
[23] J Blocki, Y Boneh, J R Nix, J Randrup, M Robel, A J Sierk and W J Swiatecki, *Ann. Phys.* **113**, 330 (1978)
[24] J P Lestone and S G McCalla, *Phys. Rev. C* **79**, 044611 (2009)
[25] P Fong, *Phys. Rev.* **102**, 434 (1956); *Phys. Rev. Lett.* **11**, 375 (1963); *Phys. Rev. C* **10**, 1122 (1974)
[26] J R Nix and W J Swiatecki, *Nucl. Phys.* **71**, 1 (1964)
[27] I I Gontchar, A E Gettinger, L V Guryan and W Wagner, *Phys. At. Nucl.* **63**, 1688 (2000)
[28] E G Ryabov, A V Karpov, P N Nadtochy and G D Adeev, *Phys. Rev. C* **78**, 044614 (2008)
[29] T Wada, Y Abe and N Carjan, *Phys. Rev. Lett.* **70**, 3538 (1993)
[30] M Brack, J Damgaard, A S Jensen, H C Pauli, V M Strutinsky and C Y Wong, *Rev. Mod. Phys.* **44**, 320 (1972)
[31] S Pal, G Chaudhuri and J Sadhukhan, *Nucl. Phys. A* **808**, 1 (2008)
[32] J Sadhukhan and S Pal, *Phys. Rev. C* **84**, 044610 (2011)
[33] J Randrup and W J Swiatecki, *Nucl. Phys. A* **429**, 105 (1984)
[34] A V Karpov, P N Nadtochy, D V Vanin and G D Adeev, *Phys. Rev. C* **63**, 054610 (2001)
[35] P N Nadtochy, G D Adeev and A V Karpov, *Phys. Rev. C* **65**, 064615 (2002)
[36] P N Nadtochy and G D Adeev, *Phys. Rev. C* **72**, 054608 (2005)
[37] P N Nadtochy, E G Ryabov, A E Gegechkori, Yu A Anischenko and G D Adeev, *Phys. Rev. C* **85**, 064619 (2012)